Q. J. R. Meteorol. Soc. (2005), **131**, pp. 1677–1693 doi: 10.1256/qj.03.210

Numerical modelling of mixed-phase frontal clouds observed during the CWVC project

By P. D. CLARK[1]*, T. W. CHOULARTON[1], P. R. A. BROWN[2], P. R. FIELD[2], A. J. ILLINGWORTH[3] and R. J. HOGAN[3]

[1]*University of Manchester Institute of Science and Technology, UK*
[2]*Met Office, Farnborough, UK*
[3]*University of Reading, UK*

(Received 19 November 2003; revised 23 September 2004)

SUMMARY

The Met Office's cloud-resolving model was used to model mixed-phase frontal clouds observed as part of the Clouds, Water Vapour and Climate programme between 1999 and 2001. The clouds were studied using the Met Office's C130 aircraft and the Chilbolton radar facility.

In the model, precipitation forms in updraughts then falls, giving rise to regions of high radar reflectivity similar to those observed. The vertical motions were driven by conditional instability or shear instability.

The sensitivity of the model results to the microphysics was examined by varying the number of primary ice nuclei and switching off the Hallett–Mossop process. It is demonstrated that the ice nucleation processes, both primary nucleation and secondary ice particle production, are key to the precipitation production in the cloud. This occurs both through the detail of cloud microphysics and the release of latent heat of fusion in the cloud. This is very sensitive to the details of the microphysics and can markedly change the cloud dynamics.

In both cases it seems that the cloud dynamics can be simulated locally without considering the large-scale forcing.

KEYWORDS: Cloud-resolving model Hallett–Mossop process

1. INTRODUCTION

At midlatitudes, frontal clouds are responsible for the bulk of the precipitation and have a significant impact on the radiation budget. Aircraft measurements (Hobbs 1974; Heymsfield 1977; Hobbs and Rango 1985; Bower *et al.* 1996) in stratiform clouds have shown that ice-particle concentrations are often far in excess of typical ice-nucleus concentrations at cloud top. This implies that some kind of ice multiplication must occur. One such mechanism which has been suggested as being responsible for generating extra ice crystals in stratiform clouds (Bower *et al.* 1996; Mason 1998) is ice-splinter production during riming (Hallett and Mossop 1974), which is known to occur in glaciating cumulus. However, this mechanism can only act in regions (which are very localized) where the vertical velocity is sufficient to maintain the supercooled liquid water. Parametrizations in many forecast and climate models assume that ice and liquid water are uniformly distributed within each grid box, and the ice/liquid-water ratio is a function of temperature alone (Smith 1990; Sundqvist 1993; Moss and Johnson 1994), ignoring the instability of mixed-phase regions where ice tends to grow at the expense of liquid water, and applying the same relationship between ice and liquid water to entirely different types of clouds. More recent parametrizations (Tremblay *et al.* 1996; Wilson and Ballard 1999) have separate variables for ice and liquid water, and use variables such as the vertical velocity to give a representation of mixed-phase clouds with a better physical basis. Considering the sensitivity of the evolution, precipitation production and radiative properties of mixed-phase clouds to their specification in models (Li and Le Treut 1992; Sun and Shine 1995; Gregory and Morris 1996; Fowler and Randell 1996), these parametrizations need to be tested against both observations and cloud-resolving models. Previous cloud-resolving model studies of mixed-phase clouds have

* Corresponding author: UMIST, PO Box 88, Manchester M60 1QD, UK.
e-mail: paul.d.clark@manchester.ac.uk

modelled cumulus (e.g. Gray 2000; Phillips *et al.* 2001) or high-latitude stratus (e.g. Jiang *et al.* 2000). This is the first such study of embedded convection within frontal stratiform clouds.

In this paper the Met Office Large-Eddy Model, described by Swann (1998), Brown (1999) and Gray *et al.* (2002), was used to model mixed-phase frontal clouds which were observed as part of the Clouds, Water Vapour and Climate (CWVC) project. Simultaneous observations by the 3 GHz radar at Chilbolton (51°12′N, 1°25′W) and the Met Office C130 aircraft in these cases, described by Hogan *et al.* (2002), have offered an intriguing glimpse of the processes that act in mixed-phase frontal clouds, but high-resolution modelling is needed to fully understand the roles of the various processes and the effect they have on the precipitation rate. Details of the instrumentation on the aircraft and how it operated in relation to the radar may be found in Hogan *et al.* (2002). Two cases were studied in detail: a cloud which extended to 4 km with embedded convection, and a deep cloud with a region with vertical motion driven by shear instability. The sensitivities of the model results to microphysics were studied by increasing or decreasing the number of primary ice nuclei by a factor of ten, and switching off the Hallett–Mossop process. Changing the microphysics affects the dynamics, since it affects the vertical distribution of latent heat release, which drives the vertical motion. Whether a particular change in the microphysics increases or decreases the maximum vertical velocity depends on how it affects the pattern of latent heating, which varies between the cases. Decreasing the number of primary ice nuclei may increase the number of ice particles where the Hallett–Mossop process is important, since it leaves more liquid water available for riming.

In section 2 we describe the model. Section 3 describes two cases in detail, comparing the model results to observations. Section 4 examines how changing the microphysics of the model affects the results. Section 5 compares and contrasts the different cases.

2. The Met Office LES model

The model used was the Met Office large-eddy simulation (LES) model. The dynamics are described in Brown (1999), and the microphysics in Swann (1998).

All the runs used the two-moment scheme for ice, snow and graupel, which has separate variables for the mass and number concentration for each species. The size distribution for each species is a gamma function. The ice variables represent the small ice particles; when the particles grow larger than 0.3 mm in diameter they are reclassified as snow. This autoconversion does not represent any physical process.

There is a single variable for water vapour and cloud liquid water. If this is greater than the saturation mixing ratio, the excess is liquid water. There is a separate variable for rain, which is formed by the melting of ice species and autoconversion from cloud water, which represents the formation of drizzle in warm clouds. However in the cases described below, the autoconversion term is zero, since the cloud water mixing ratio never reaches the threshold.

The model is initialized with profiles of potential temperature, total water (as relative humidity) and horizontal wind, based on measurements taken by the C130 aircraft, with radiosonde data for higher levels. Horizontal inhomogeneities such as convection are allowed to develop by applying a random temperature perturbation between ± 0.1 °C throughout the domain.

The model was run in a two-dimensional (2D) (y–z) configuration with 100 m resolution in the horizontal and the vertical with 256 points in the horizontal.

The domain is periodic in the horizontal. No large-scale ascent or descent is included in the model.

Following Yin *et al.* (2000), the radar reflectivity (dB) is given by

$$Z = 10 \log \sum_x \int_0^\infty \mathrm{d}D \, n_x(D) \frac{|K|^2}{|K_1|^2} D^6, \tag{1}$$

where $n_x(D)$ is the number concentration (m^{-3}) of each species (rainwater, ice, snow and graupel) with diameter D (mm), $|K_1|^2 = 0.93$ is the dielectric factor of liquid water and $|K|^2$ is the dielectric factor of the particle. For the ice species, this is given by

$$|K|^2 = |K_\mathrm{i}|^2 \frac{\rho^2}{\rho_\mathrm{i}^2}, \tag{2}$$

where $|K_\mathrm{i}|^2 = 0.174$ is the dielectric factor of solid ice, $\rho_\mathrm{i} = 910$ kg m^{-3} is the density of solid ice and ρ is the density of the particle, taken as 800 kg m^{-3} for ice, 100 kg m^{-3} for snow and 300 kg m^{-3} for graupel. This calculation cannot model the bright band in the melting layer, which is caused by ice particles coated with liquid water. Because the radar reflectivity depends on the sixth power of the size, it is sensitive to the microphysics. The cloud water is ignored since the droplets are too small to have a significant effect. Since the model has a single-moment scheme for the rainwater, the size distribution is parametrized as in Swann (1998).

The microphysical parametrization used in the model is not sophisticated enough to make it possible to calculate differential radar reflectivity. To do that it would be necessary to distinguish between pristine ice crystals and aggregates, and between columns and plates, and to describe the axis ratio and orientation of each species as a function of size.

Primary ice nucleation uses the parametrization of Meyers *et al.* (1992). The number of ice particles per cubic metre is allowed to increase until it reaches a value given by

$$N_\mathrm{i} = \exp(12.96 S_\mathrm{i} - 6.69), \tag{3}$$

where S_i is the supersaturation with respect to ice; primary nucleation only occurs when the supersaturation is increasing.

In the model the Hallett–Mossop process occurs as a result of both snow and graupel riming, with the number of splinters produced given by

$$N_\mathrm{HM} = \begin{cases} 350 \, m_\mathrm{R}(1 - |T + 5|/2.5) & \text{for } -7.5 < T < -2.5 \\ 0 & \text{otherwise,} \end{cases} \tag{4}$$

where m_R is the mass (mg) of rime and T is the temperature (°C). Since the model contains no information about the cloud droplet spectrum, we cannot employ any of the dependencies observed in laboratory experiments (e.g. on the concentration of droplets larger than 24 μm, or on the relative velocity of cloud droplet and the rimer particle). Since it would take time for the droplets to grow to 24 μm, it would seem that the model might overestimate the number of ice particles produced.

For each case, a control run was carried out with the Hallett–Mossop process and the standard rate of primary ice nucleation. To test the sensitivity of the results to microphysics, further runs were carried out without the Hallett–Mossop process, and with the number of primary ice nuclei increased and decreased by a factor of 10, which is typical of the range of uncertainty in ice nucleus concentration.

3. Results

In both the cases, spin-up lasts between twenty minutes and half an hour. During spin-up, the maximum vertical velocity increases from zero and the total liquid and ice water both approach a steady value. After that, the vertical velocity oscillates as individual thermals grow and decay for the next hour or so. The results shown are at one hour into the runs.

(*a*) *Flight A661 (30 March 1999)*

Flight A661, described in Hogan *et al.* (2002), is a case-study of a warm-frontal mixed-phase cloud. At the time of the flight, there was a warm front over the south of the UK. This was associated with light stratiform precipitation of around 1 mm hr^{-1} observed by the operational radar network.

During the flight, aircraft profiles were taken from the surface to 4500 m, but they were not in the region where the updraughts were observed. In the altitude range of the cloud layer, the model is initialized by interpolating run-mean temperature and wind components from horizontal flight legs. The aircraft vertical profiles provide data below cloud base. Figure 1 shows the initial profiles of horizontal velocity, temperature and total water mixing ratio. The cloud extends from 1 km to 4 km, with cloud base at 2 °C and cloud top at −16 °C. The top of the model is at 7 km. To prevent spurious reflection of gravity waves at the upper boundary, a damping layer is included near the top of the model, where the velocity, potential temperature and water mixing ratio are relaxed towards their zonal mean values above 6 km.

Figure 2 shows the radar reflectivity, vertical velocity and mixing ratios of ice and liquid water for the control run. These plots are restricted in horizontal extent to show the main updraught, which extends across the boundary of the domain. At any time there were two or three updraughts, and individual updraughts lasted for about half an hour. The non-zero radar reflectivity below cloud base is due to rain (not included in the liquid water field).

The vertical velocity shows the features identified in Hogan *et al.* (2002), with Kelvin–Helmholtz instability near the melting layer at 1.5 km and updraughts above, which slant due to the shear. The maximum vertical velocity is about 1.2 m s^{-1}, which is comparable to the observations.

To test the importance of the Kelvin–Helmholtz instability, a run was carried out with the initial horizontal velocity set to zero. In that case there was very little vertical motion. It appears that the Kelvin–Helmholtz instability creates disturbances at 1.5 km, which grow as they rise by conditional instability.

As in the observations, the maximum liquid water content at each level in the updraughts is upshear of the maximum ice content. In the model, the ice particles fall, whereas the cloud water does not. In the real cloud, the ice particles are bigger than the water droplets, so they fall faster.

The largest values of rainwater mixing ratio (not shown) occur below the updraughts, with a maximum of 0.25 g kg^{-1}, with stratiform rain from the rest of the cloud giving an average rainfall rate of 1.2 mm $hour^{-1}$. The rain is produced by melting of ice rather than from cloud water by the autoconversion term, since the liquid water mixing ratio never reaches the threshold for autoconversion.

The radar reflectivity shows strong signals in the updraught, with a maximum of about 30 dBZ, similar to the observations shown in Hogan *et al.* (2002).

In addition to the liquid water in the convective updraught cores, there is also liquid water at cloud top, which does not appear in Fig. 2(d) since it is less than the lowest

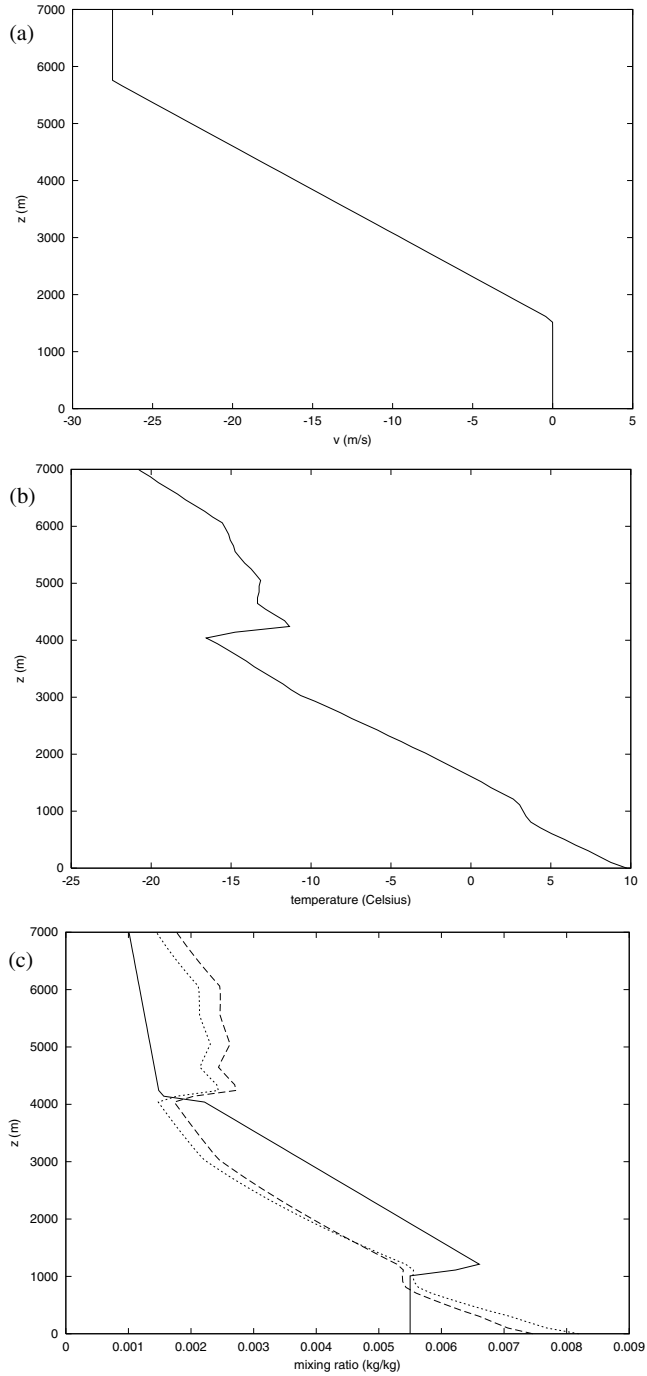

Figure 1. Flight A661 initial profiles of (a) horizontal velocity, (b) temperature and (c) total water mixing ratio. In (c), the saturation mixing ratios over water (dashed) and over ice (dotted) are also shown.

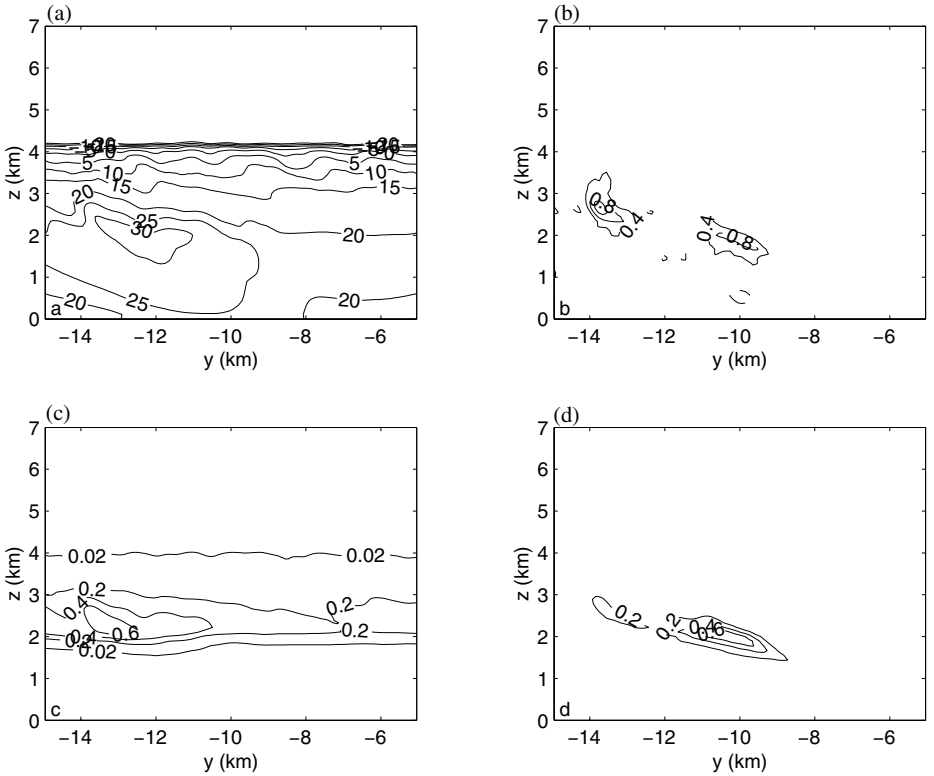

Figure 2. LES model output after one hour from the control run for flight A661: (a) radar reflectivity (dBZ) from −20 to +30, with contour interval 10, (b) vertical velocity (m s^{-1}) with contour interval 0.4, zero contour omitted, and negative contours dashed, (c) total ice mixing ratio (g kg^{-1}), with contour interval 0.2, and 0.02 contour added to show the extent of the cloud, and (d) liquid water mixing ratio (g kg^{-1}) with contour interval 0.2.

contour level. This occurs because, at the cloud-top temperature, the number of ice nuclei is insufficient to take up vapour and so the air is supersaturated with respect to liquid water.

(*b*) *Flight A806 (21 November 2000)*

The observations from this case were described by Field *et al.* (2004). A warm front was occluding as it moved into the south-west of the UK, and a broad band of precipitation swept across southern England from the south-west. Rain was first measured at Chilbolton at 1345 UTC. In this case, the radar showed cloud extending from just above the ground to about 8 km, with fallstreaks in the ice in the first 4 km, above the melting layer. The initial vertical profile taken by the aeroplane shows mainly liquid water below the freezing level at 2 km, with mixed-phase cloud above that; the maximum liquid water mixing ratio is about 0.7 g kg^{-1}. From animations of the radar reflectivity, it appears that large ice particles first form in areas about 1 km across at about 4 km, and merge into wider fallstreaks as they fall.

These fallstreaks do not have values of differential radar reflectivity significantly different from those in the rest of the cloud, unlike flight A661. The horizontal flight legs by the aircraft, at 3 km, 3.5 km and 4 km, show that they contain more liquid water than the surrounding cloud; the maximum liquid water mixing ratio is 0.15 g kg^{-1}

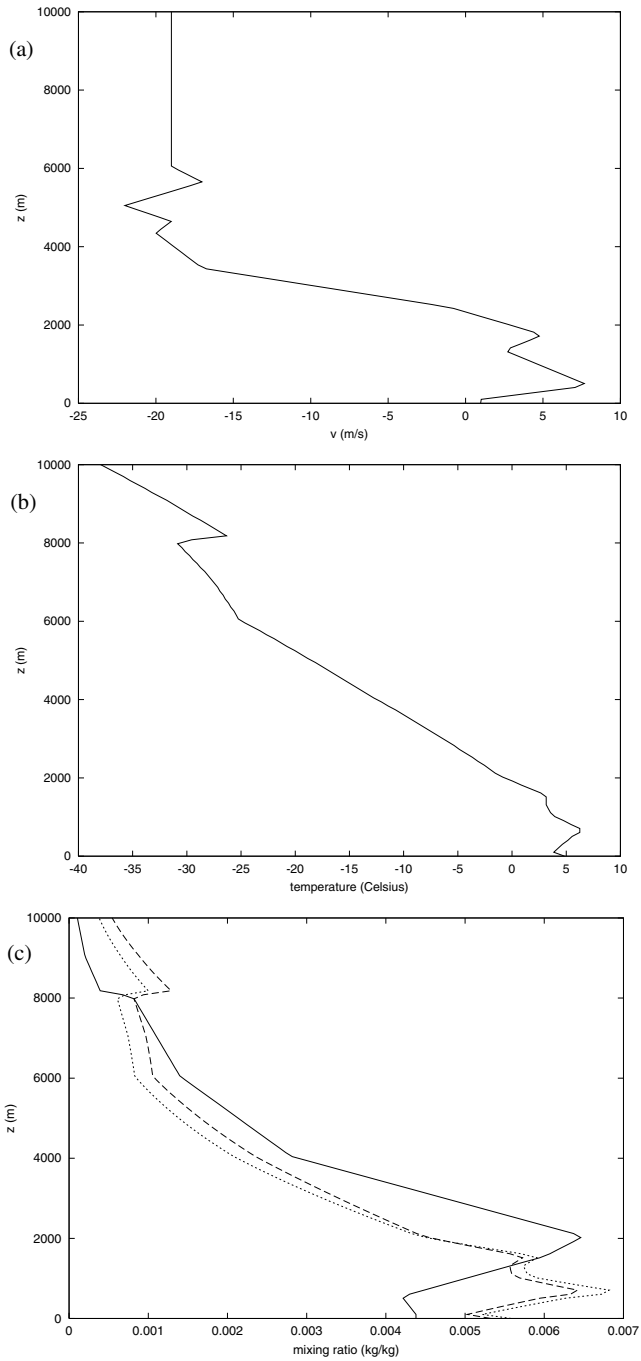

Figure 3. As Fig. 1, but for flight A806.

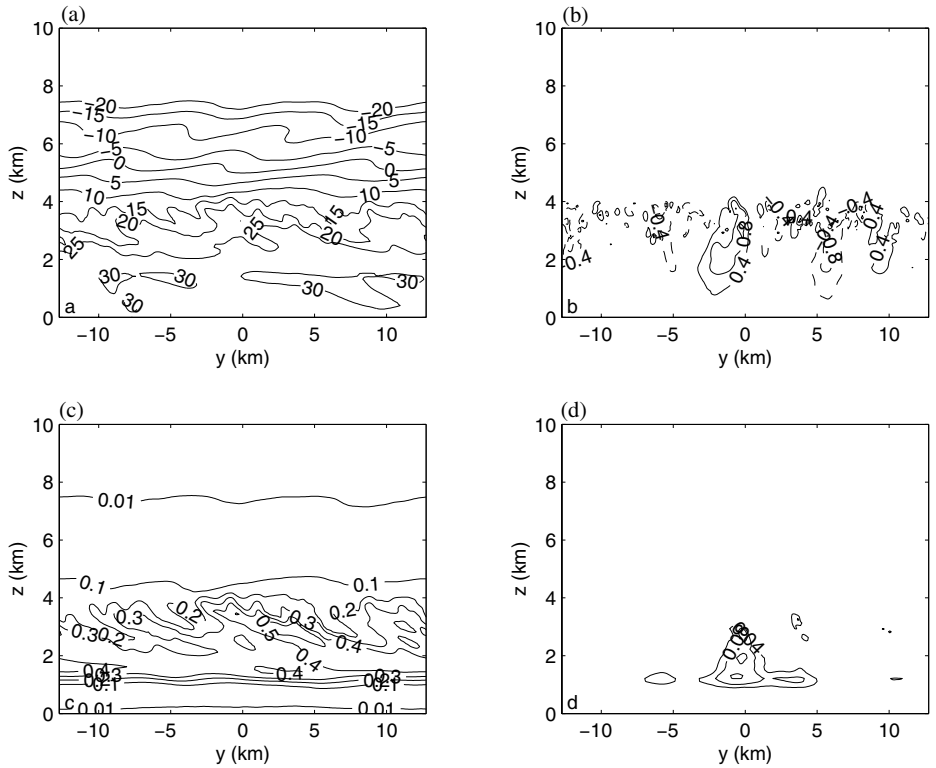

Figure 4. As Fig. 2, but for flight A806. Contour intervals in (a) and (b) are as before, but (c) has interval 0.1 g kg^{-1} with extra contour 0.01 and (d) has interval 0.04 g kg^{-1}.

compared with less than 0.02 g kg^{-1} outside the fallstreaks. The maximum vertical velocity measured in these flight legs was about 1.3 m s^{-1}.

The initial condition is based on an aircraft sounding up to about 6 km, with radiosonde data above that height. Figure 3 shows the initial profiles of horizontal velocity, temperature and total water mixing ratio. The cloud extends from 1.5 km to 8 km, with cloud base at 5 °C and cloud top at −31 °C, and the top of the model was at 10 km. Spurious reflections of gravity waves at the upper boundary are prevented by relaxing the velocity, potential temperature and water mixing ratio towards their zonal mean values above 8.5 km.

Figure 4 shows the radar reflectivity, vertical velocity and mixing ratios of ice and liquid water for the control run. The vertical velocity shows features which are about 1 km across at around 4 km, which is where the greatest vertical shear in the initial profile occurs. These appear to be Kelvin–Helmholtz billows. Snow forms in the updraughts, then merges to form wider regions as it falls. These slope due to the shear, giving rise to a pattern similar to the radar observations.

The vertical motions below 4 km are driven by conditional instability modified by the precipitation. As ice particles fall through this region, they grow by vapour deposition, releasing latent heat, which drives updraughts. In a simulation with the fallout of precipitation turned off, the updraughts below 4 km were much weaker, with a maximum vertical velocity of 0.2 m s^{-1}.

Liquid water occurs at cloud base, and in the strongest updraught below 4 km, which is centred at $y = -2$ km.

TABLE 1. FLIGHT A661: ROOT-MEAN-SQUARE VERTICAL VELOCITY, MAXIMUM RADAR REFLECTIVITY AND MAXIMUM ICE NUMBER CONCENTRATIONS FROM OBSERVATIONS AND FROM LES RUNS

	r.m.s. w (m s^{-1})	Max. Z (dBZ)	Max. ice no. (l^{-1})
Observations	0.52	30	2500
Control	0.56	30	65
No Hallett–Mossop	0.45	31	3
10× ice nuclei	0.54	38	60
0.1× ice nuclei	0.65	41	150

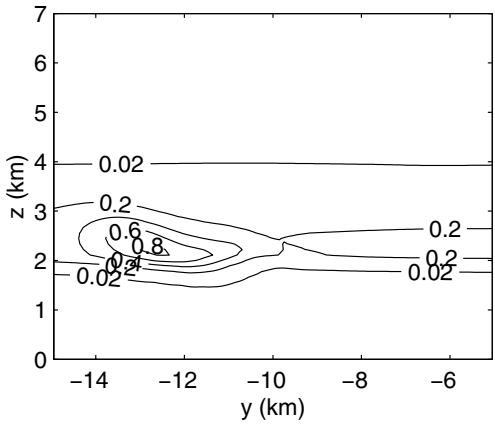

Figure 5. Total ice mixing ratio (g kg^{-1}) for flight A661: LES model run without the Hallett–Mossop process.

In this case, there is no liquid water at cloud top in the observations or the control run, due to the lower temperatures than flight A661. In the model there is liquid water at cloud base, which is above the freezing point, and in the updraughts, both in the Kelvin–Helmholtz region and the conditionally unstable region.

4. SENSITIVITY TESTS

(*a*) *Flight A661 (30 March 1999)*

Table 1 summarizes the differences between the runs with and without the Hallett–Mossop process and the runs with different primary ice nuclei concentrations. For the observations, the root-mean-square (r.m.s.) vertical velocity for each horizontal leg of the flight was calculated, and the maximum is shown. For the model runs, the r.m.s. vertical velocity at each level was calculated, and the maximum is shown. In the control run, the maximum ice number concentration and radar reflectivity both occur in the updraught, and they are used as a test of the microphysics in the updraught.

Figure 5 shows the mixing ratio of ice for the run without the Hallett–Mossop process, which shows the largest difference from the control. The maximum mixing ratio is larger than for the control run. During spin-up, in the control run the Hallett–Mossop process creates more ice particles, which grow by vapour deposition, so when the updraught forms there is less water vapour available to form ice.

Switching off the Hallett–Mossop process decreases the number of ice particles by a factor of 20, suggesting that the Hallett–Mossop process is the dominant source of ice nuclei in the updraught in this case. In the non-Hallett–Mossop run the small ice

particles are relatively uniformly distributed in the horizontal, whereas in the Hallett–Mossop run it occurs mainly in the updraught. This is because liquid water occurs mainly in the updraught, so the Hallett–Mossop process is significant there. The largest ice number concentration occurred in the run where the number of primary ice nuclei was decreased, showing that the Hallett–Mossop process increases the number of ice particles in this case. Even in that case, the number is still much smaller than in the observations. The observed ice number concentration is measured with the 2D-C probe (described in Hogan *et al.* 2002), and is likely to be an underestimate due to the probe undercounting crystals smaller than 100 μm. In Phillips *et al.* (2002), this case was modelled using a model with explicit microphysics, which produced the number of ice crystals seen in the observations. In this model the splinters produced by the Hallett–Mossop process cause water droplets to freeze by contact nucleation, producing ice particles which can rime and produce more splinters by the Hallett–Mossop process. This mechanism is not captured by the LES, since contact nucleation produces small ice particles, which do not produce Hallett–Mossop splinters when they rime.

The highest r.m.s. vertical velocity also occurs in the run where the number of primary ice nuclei was decreased, and the run where the number of primary ice nuclei was increased has smaller r.m.s. velocity than the control. In this case, the vertical motion is driven by the release of latent heat.

The run where the number of primary ice nuclei was increased has the earliest onset of precipitation, and the highest maximum precipitation rate. In the other runs, precipitation starts at about the same time, but the run without the Hallett–Mossop process has the smallest maximum precipitation rate.

Decreasing and increasing the number of primary ice nuclei both increase the maximum radar reflectivity. The former increases it in the updraught by increasing the size of the ice particles, whereas the latter increases it in the rain below the updraught.

For this case we also investigated sensitivity to model resolution, to test whether the resolution used was sufficient. The run with 50 m horizontal resolution gives similar results to the standard run. At 200 m horizontal resolution, the updraughts are weaker, and at 500 m horizontal resolution, there were no updraughts. Changing the vertical resolution to 50 m or 200 m made little difference to the results. Increasing the vertical resolution to 400 m reduces the maximum vertical velocity to 0.35 m s^{-1}. Increasing the vertical resolution to 1 km reduces the maximum vertical velocity to less than 0.05 m s^{-1}, and the water fields are approximately horizontally uniform.

In version 2.3 of the Met. Office's LES, contributions of different microphysical processes to the rates of change of the various water species can be written out, as described in Gray *et al.* (2002). The graphs show a thirty-minute average one hour into the model runs, after the model has spun up. They do not include rates of change due to advection and falling of hydrometeors. Processes with negligible contributions to the latent heating have been omitted for clarity, which include all processes involving graupel. Since they show horizontal averages, sublimation and vapour deposition can occur at the same level. Figure 6 shows the contributions from various physical processes to the latent heating for the control run, with positive values corresponding to release of latent heat. Table 2 is a key to the terms included in the figure.

Primary ice nucleation and the Hallett–Mossop process do not contribute significantly to the latent heat budget, since the total mass of the particles produced is small. At the top of the cloud, the main contribution is from the growth of ice by vapour deposition. In the body of the cloud, in the updraughts latent heat is released by vapour deposition onto snow with a smaller contribution from snow accumulating liquid water,

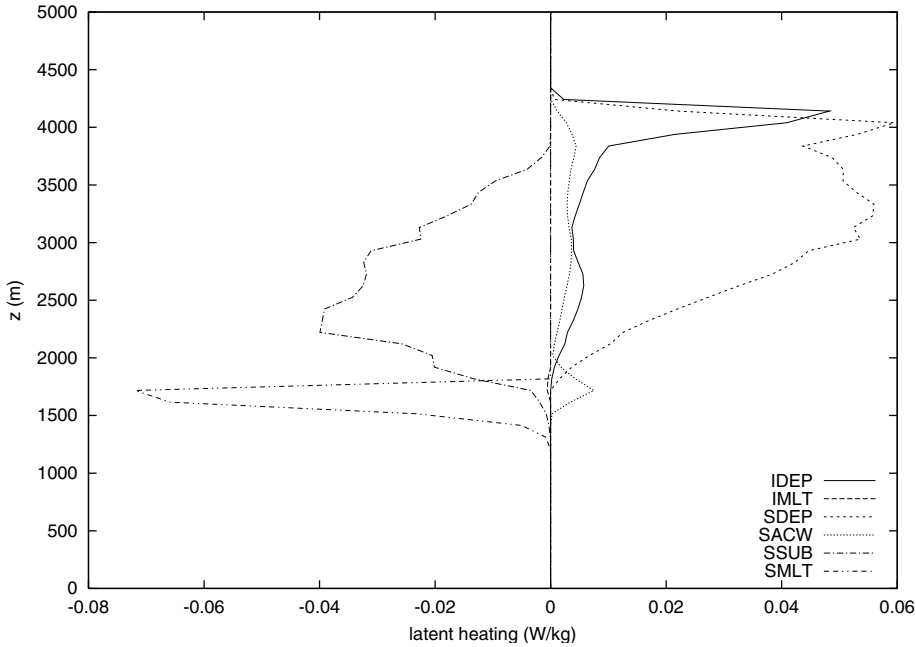

Figure 6. Contributions to latent heating from microphysical processes for the LES control run for flight A661. The abbreviations are defined in Table 2.

TABLE 2. BUDGET TERMS: MICROPHYSICAL PROCESSES MAKING SIGNIFICANT CONTRIBUTIONS TO THE LATENT HEATING

Term	Source	Sink	Description
IDEP	ice	vapour	Growth of ice by vapour deposition
IMLT	rain	ice	Melting of ice
SDEP	snow	vapour	Growth of snow by vapour deposition
SACW	snow	water	Snow accumulating liquid water
SSUB	vapour	snow	Sublimation of snow
SMLT	rain	snow	Melting of snow

and in the downdraughts latent heat is taken up by the sublimation of snow. This helps to drive the vertical motion. In the melting layer at 1.5 km, latent heat is taken up by melting snow.

Figure 7 shows the difference between contributions to latent heating for the run without the Hallett–Mossop process and the control run, with positive values corresponding to more latent heat release or less latent heat uptake in the run without the Hallett–Mossop process. Since there are fewer small ice particles in the updraughts below 3 km in the run without the Hallett–Mossop process, there is less vapour deposition onto the ice there. Also there is less snow throughout the cloud, so less vapour deposition in the updraughts and sublimation in the downdraughts. These changes make the updraughts cooler and the downdraughts warmer in the control run, which weakens the vertical motion.

(*b*) *Flight A806 (21 November 2000)*

Table 3 summarizes the differences between the runs with and without the Hallett–Mossop process and the runs with different primary ice nuclei concentrations for this

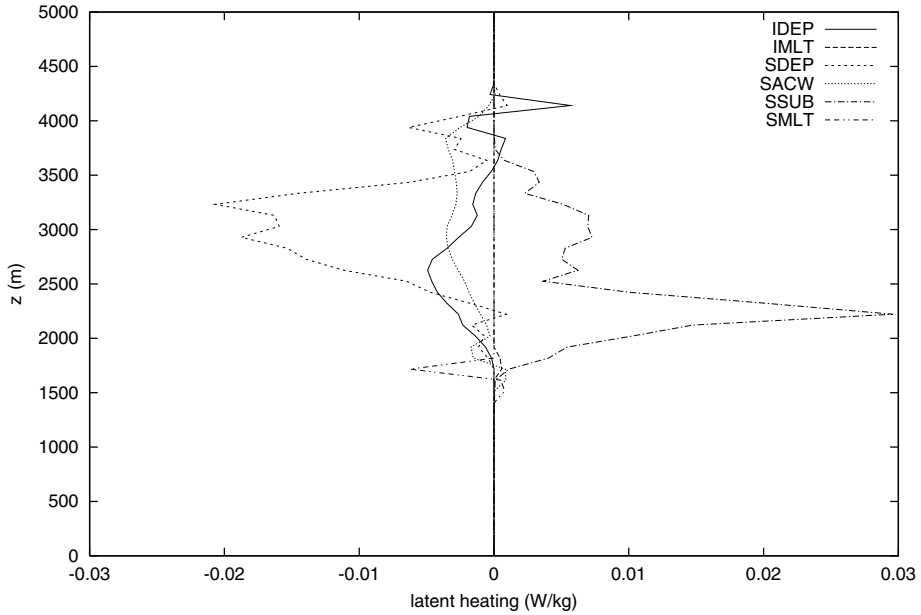

Figure 7. Contributions to latent heating from microphysical processes for flight A661: differences between the LES run without the Hallett–Mossop process and the control run.

TABLE 3. AS TABLE 1, BUT FOR FLIGHT A806

	r.m.s. w (m s^{-1})	Max Z (dBZ)	Max ice no. (l^{-1})
Observations	0.67	30	65
Control	0.58	32	47
No Hallett–Mossop	0.59	33	47
10× ice nuclei	1.15	31	500
0.1× ice nuclei	0.87	41	14

case. Figure 8 shows the mixing ratios of ice and liquid water for the run with reduced primary ice nuclei, which shows the largest difference from the control.

In this case, switching off the Hallett–Mossop process makes very little difference to the results since the cloud-top temperature is so low that there is sufficient primary ice nucleation to cause nearly all the condensed water to freeze except in the updraught, so there is little riming.

The largest value of the ice number concentration occurs in the run where the number of primary ice nuclei has been increased, and the smallest ice number concentration occurs when the number of primary ice nuclei is decreased.

The radar reflectivity is largest in the run where the number of primary ice nuclei has been decreased, since decreasing the number of ice particles increases their size. Conversely the radar reflectivity is smallest in the run where the number of primary ice nuclei has been increased, since increasing the number of ice particles decreases their size.

The run where the number of primary ice nuclei was decreased has larger r.m.s. vertical velocity than the control, but the highest r.m.s. vertical velocity occurs in the run where the number of primary ice nuclei was increased.

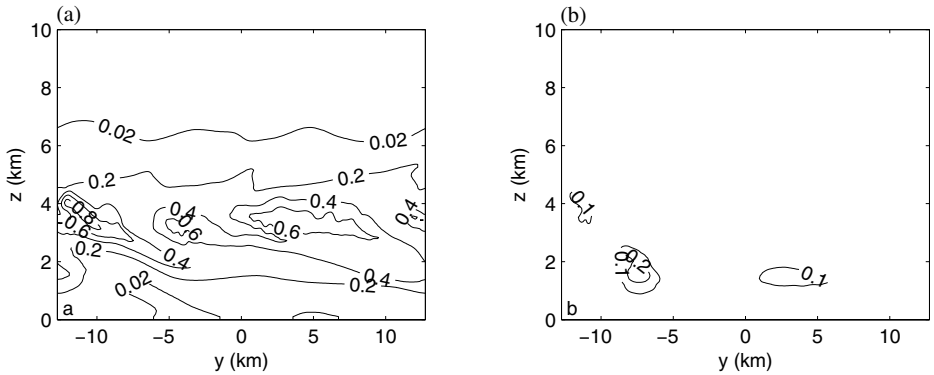

Figure 8. LES model output for flight A806 with reduced primary ice nuclei: (a) total ice mixing ratio and (b) liquid water mixing ratio (both g kg^{-1}).

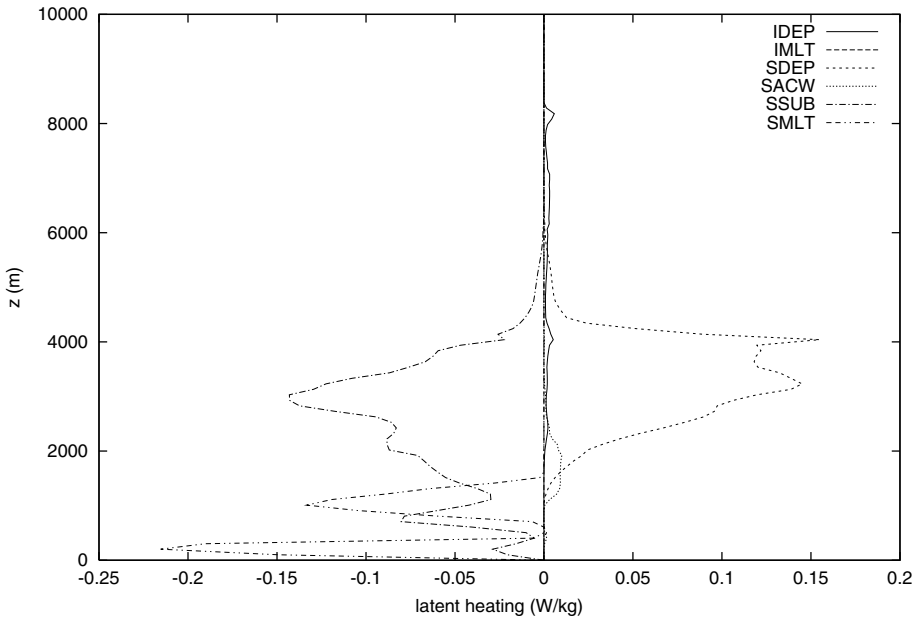

Figure 9. As Fig. 6, but for flight A806.

In the run where the number of primary ice nuclei was increased, there is no liquid water in the Kelvin–Helmholtz region. The ice particles are more numerous and smaller than in the control run, so they have a greater surface area, making them more efficient at collecting water vapour. As a result, water vapour does not reach saturation with respect to liquid water in this region.

The run where the number of primary ice nuclei was increased has the earliest onset of precipitation, and the run where the number of primary ice nuclei was decreased has the latest onset of precipitation, and this latter run has the highest maximum precipitation rate. The maximum precipitation rate is about the same in the other three runs.

Figure 9 shows the contributions from various physical processes to the latent heating for the control run. At the top of the cloud, the main contribution is from the

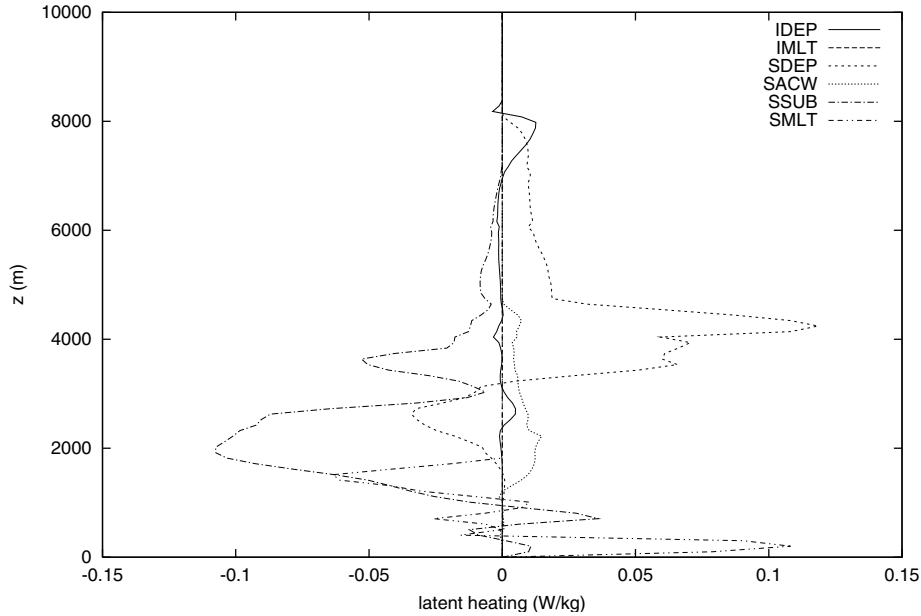

Figure 10. Contributions to latent heating from microphysical processes for flight A806: differences between the LES run with reduced primary ice nucleation and the control run.

growth of ice by vapour deposition. In the body of the cloud, particularly below 4 km, in the updraughts latent heat is released by vapour deposition onto snow with a much smaller contribution from snow accumulating liquid water around 2 km, and in the downdraughts latent heat is taken up by the sublimation of snow. This helps to drive the vertical motion. In the melting layer at 1 km, latent heat is taken up by melting snow.

Figure 10 shows the difference between contributions to latent heating for the run with reduced primary ice nucleation and the control run. Reducing the number of primary ice nuclei decreases the number of ice particles and hence the uptake of water vapour by deposition, leaving more water vapour in the background cloud. Also there is more liquid water in the updraughts, with supercooled liquid water up to 4 km. This leads to more deposition and accretion in the updraughts, hence more latent heat release and hence stronger updraughts and highest maximum precipitation rate.

5. Conclusions

In both the cases described above, precipitation forms in updraughts, which are driven by a combination of conditional instability and latent heat release in A661, and by shear instability in A806. In both cases the precipitation reaches the ground as rain.

The radar reflectivities from the model show reasonable agreement with observations, considering the sensitivity to the size of particles and the relatively crude microphysics in the model. The horizontal extent of features and the way that fall streaks merge as they fall in A806 are also captured well.

As in the observations, in the sheared updraughts in A661 the maximum ice concentration occurs downshear of the maximum liquid water concentration. In the model, this occurs because the ice falls whereas the cloud liquid water does not,

so in each vertical profile the maximum ice concentration is below the maximum liquid water concentration. In the real cloud, the ice particles are larger than the liquid water droplets, and fall faster.

Halving the horizontal or vertical grid spacing has little effect on the results, showing that the resolution used is sufficient. Decreasing the horizontal or vertical resolution weakens the convection, and stops it entirely at very coarse resolutions.

Switching off the Hallett–Mossop process affects the background cloud as well as the updraughts, even when there is no liquid water there, since the model is initialized with a liquid water cloud, which becomes glaciated during spin-up.

In A661, switching off the Hallett–Mossop process has the largest effect of any of the sensitivity tests carried out, as it is the main source of ice nuclei in the control run.

In A806, switching off the Hallett–Mossop process has little effect on the results. This is because the low cloud-top temperature results in large numbers of primary ice crystals, and there is little liquid water in the parts of the cloud in the temperature range where the Hallett–Mossop process occurs.

Changing the microphysics in the LES also changes the dynamics of the runs. Increasing the number of primary ice nuclei can either increase or decrease the velocity in the updraughts, depending on where the latent heat is released.

In both cases, decreasing the number of primary ice nuclei increases the maximum updraught velocity, since it results in more water vapour in the background cloud, leading to more vapour deposition and hence more latent heat release in the updraughts. This also results in more precipitation.

Increasing the number of primary ice nuclei reduces the amount of liquid water, since it results in more numerous, smaller ice particles, which are more efficient at collecting water vapour.

Decreasing the number of primary ice nuclei may actually increase the number of ice particles if the Hallett–Mossop process is the dominant source of ice nuclei, since this may give rise to more liquid water in the region where the Hallett–Mossop process takes place. Conversely, increasing the number of primary ice nuclei may decrease the number of ice particles by reducing the amount of liquid water in the region where the Hallett–Mossop process takes place. This is what happens in the updraughts in A661.

In A806 the number of ice particles in the cloud is dominated by primary nucleation with secondary ice particles playing a lesser role. The Hallett–Mossop effect becomes more important when the number of primary ice nuclei is reduced, which results in higher liquid water content and hence more riming.

In both cases the standard version of the model's microphysics produces results closest to the observations. However the parametrization of primary ice nucleation in the model is unrealistic, with extra ice particles being produced whenever the supersaturation with respect to ice is increasing. A more realistic parametrization would require a tracer variable for the ice nuclei, which could be reduced when ice particles form and increased when they sublime. To know the number of ice nuclei in the observed clouds, it would be necessary to sample the air before the clouds form in it. Also the production of extra ice particles as snow breaks up during sublimation is not included in the model.

Consistent with observations, A661 has a supercooled liquid water layer at cloud top and A806 does not. This is simply because in the case of A806 there are sufficient ice particles high in the cloud to prevent liquid water from being produced.

In both cases the vertical motion decays after about two hours, as the instability which drives them is dissipated. To maintain the motion for longer periods would require large-scale forcing. However it is apparent that the main features of the cloud

can be produced by considering the local dynamics as modelled by the LES. The role of the large-scale dynamics seems to be to provide the appropriate thermodynamic environment.

References

Bower, K. N., Moss, S. J., Johnson, D. W., Choularton, T. W., Latham, J., Brown, P. R. A., Blyth, A. M. and Cardwell, J. 1996 A parametrization of the ice water content observed in frontal and convective clouds. *Q. J. R. Meteorol. Soc.*, **122,** 1815–1844

Brown, A. R. 1999 The sensitivity of large-eddy simulations of shallow cumulus convection to resolution and subgrid model. *Q. J. R. Meteorol. Soc.*, **125,** 469–482

Field, P. R., Hogan, R. J., Brown, P. R. A., Illingworth, A. J., Choularton, T. W., Kaye, P. H., Hirst, E. and Greenaway, R. 2004 Simultaneous radar and aircraft observations of mixed-phase cloud at the 100 m scale. *Q. J. R. Meteorol. Soc.*, **130,** 1877–1904

Fowler, L. D. and Randell, D. A. 1996 Liquid and ice cloud microphysics in the CSU general circulation model: 3. Sensitivity to modeling assumptions. *J. Climate*, **9,** 561–586

Gray, M. E. B. 2000 Characteristics of numerically simulated mesoscale convective systems and their application to parameterization. *J. Atmos. Sci.*, **57,** 3953–3970

Gray, M. E. B., Petch, J., Derbyshire, S. H., Brown, A. R., Lock, A. P., Swann, H. A. and Brown, P. R. A. 2002 'Version 2.3 of the Met Office Large Eddy Model, Part II: Scientific documentation'. Turbulence and Diffusion Note 276, Met Office, Exeter, UK

Gregory, D. and Morris, D. 1996 The sensitivity of climate simulations to the specification of mixed-phase clouds. *Clim. Dyn.*, **12,** 641–651

Hallett, J. and Mossop, S. C. 1974 Production of secondary ice particles during the riming process. *Nature*, **249,** 26–28

Heymsfield, A. J. 1977 Precipitation development in stratiform ice clouds: A microphysical and dynamical study. *J. Atmos. Sci.*, **34,** 367–381

Hobbs, P. V. 1974 High concentration of ice particles in a layer cloud. *Nature*, **251,** 694–696

Hobbs, P. V. and Rango, A. L. 1985 Ice particle concentrations in clouds. *J. Atmos. Sci.*, **42,** 2523–2549

Hogan, R. J., Field, P. R., Illingworth, A. J., Cotton, R. J. and Choularton, T. W. 2002 Properties of embedded convection in warm-frontal mixed-phase cloud from aircraft and polarimetric radar. *Q. J. R. Meteorol. Soc.*, **128,** 451–476

Jiang, H. L. ,Cotton, W. R., Pinto, J. O., Curry, J. A. and Weissbluth, M. J. 2000 Cloud resolving simulations of mixed-phase Arctic stratus observed during BASE: Sensitivity to concentration of ice crystals and large-scale heat and moisture advection. *J. Atmos. Sci.*, **57,** 2105–2117

Li, Z.-X. and Le Treut, H. 1992 Cloud-radiation feedbacks in a general circulation model and their dependence on cloud modelling assumptions. *Clim. Dyn.*, **7,** 133–139

Mason, B. J. 1998 The production of high ice-crystal concentrations in stratiform clouds. *Q. J. R. Meteorol. Soc.*, **124,** 353–356

Meyers, M. P., Demott, P. J. and Cotton, W. R. 1992 New primary ice-nucleation parameterizations in an explicit cloud model. *J. Appl. Meteorol.*, **31,** 708–721

Moss, S. J. and Johnson, D. W. 1994 Aircraft measurements to validate and improve numerical model parameterizations of ice to water ratios in clouds. *Atmos. Res.*, **34,** 1–25

Phillips, V. T. J., Blyth, A. M., Brown, P. R. A., Choularton, T. W. and Latham, J. 2001 The glaciation of a cumulus cloud over New Mexico. *Q. J. R. Meteorol. Soc.*, **127,** 1513–1534

Phillips, V. T. J., Choularton, T. W., Blyth, A. M. and Latham, J. 2002 The influence of aerosol concentrations on the glaciation and precipitation of a cumulus cloud. *Q. J. R. Meteorol. Soc.*, **128,** 951–971

Smith, R. N. B. 1990 A scheme for predicting layer clouds and their water content in a general circulation model. *Q. J. R. Meteorol. Soc.*, **116,** 435–460

Sun, Z. and Shine, K. P. 1995 Parameterization of ice cloud radiative properties and its applications to the potential climatic importance of mixed-phase clouds. *J. Climate*, **8,** 1874–1888

Sundqvist, H. 1993 Inclusion of ice phase hydrometeors in cloud parameterization for mesoscale and large-scale models. *Beitr. Phys. Atmos.*, **66,** 137–147

Swann, H. 1998 Sensitivity to the representation of precipitating ice in CRM simulations of deep convection. *Atmos. Res.*, **47–48,** 415–435

Tremblay, A., Glazier, A., Yu, W. and Benoit, R. 1996 A mixed-phase cloud scheme based on a single prognostic equation. *Tellus*, **48,** 483–500

Wilson, D. R. and Ballard, S. P. 1999 A microphysically based precipitation scheme for the UK Meteorological Office Unified Model. *Q. J. R. Meteorol. Soc.*, **125,** 1607–1636

Yin, Y., Levin, Z., Reisin, T. G. and Tzivion, S. 2000 The effects of giant cloud condensation nuclei on the development of precipitation in convective clouds—a numerical study. *Atmos. Res.*, **53,** 91–116